Defining optimal axial and lateral resolution for estimating scatterer properties from volumes using ultrasound backscatter

Michael L. Oelze[a] and William D. O'Brien, Jr.
Bioacoustics Research Laboratory, Department of Electrical and Computer Engineering, University of Illinois, 405 North Mathews, Urbana, Illinois 61801

(Received 25 June 2003; revised 6 March 2004; accepted 19 March 2004)

The rf signals used to construct conventional ultrasound B-mode images contain frequency-dependent information that can be examined through the backscattered power spectrum. Typically, the backscattered power spectrum is calculated from a region of interest (ROI) within some larger volume. The dimensions of the ROI are defined axially by the spatial length corresponding to the time gate and laterally by the number of scan lines included in the ROI. Averaging the backscattered power spectra from several independent scan lines can reduce the presence of noise caused by electronics and by the random scatterer spacings, but also decreases the lateral resolution of the interrogation region. Furthermore, larger axial gate lengths can be used to reduce the effects of noise and improve the precision and accuracy of scatterer property estimates but also decreases the axial resolution. A trade-off exists between the size of the ROI (the number of scan lines used, the separation distance between each scan line, the axial gate length) and the accuracy and precision of scatterer property estimates. A series of simulations and measurements from physical phantoms were employed to examine these trade-offs. The simulations and phantom measurements indicated the optimal lateral and axial sizes of the ROI, where estimate accuracy and precision were better than 10% and 5%, respectively, occurred at 4 to 5 beamwidths laterally and 15 to 20 spatial pulse lengths axially. © *2004 Acoustical Society of America.*
[DOI: 10.1121/1.1739484]

PACS numbers: 43.80.Qf, 43.80.Vj [FD] Pages: 3226–3234

I. INTRODUCTION

A conventional B-mode image is made up of several parallel or consecutively spaced axial rf time signals. Each rf time signal is a series of echoes backscattered from structures in the interrogated medium. In a conventional B-mode image, the frequency-dependent information in an rf time signal is not utilized. Instead, conventional B-mode images of tissues using ultrasound are made by generating a gray-scale image using the envelope-detected rf signal backscattered from the tissues.

The frequency-dependent information in an rf time signal may be related to the tissue microstructure (structures less than the ultrasound wavelength).[1–13] Parametrizing the frequency-dependent information of backscattered signals from tissues allows the characterization and differentiation of tissues. Several researchers have used quantitative ultrasound (QUS) or parameter information about the shape of the spectrum of scattered ultrasound to classify tissue microstructure and identify disease.[2,9,11–16] Other researchers have been able to estimate the size, shape, and internal make-up of scatterers in tissues from models.[3,5–7,9–11,16]

Scattering from tissues is often modeled using the Born approximation (weak scattering with no multiple scattering).[17] Regions of interest (ROIs) are chosen from interrogated volumes, and the spectral properties of the rf signal corresponding to the ROIs are quantified and related to models of tissue scattering. Tissue scattering often represents a stochastic process that gives rise to incoherent and coherent spectra.[17–19] The incoherent spectrum includes information about the size, shape, density, and mechanical properties of the scatterers.[19] If a model accurately describes the incoherent spectrum, then estimates of scatterer properties can be made. The coherent part of the spectrum is also a function of the individual scatterer properties but is strongly dependent on the spatial variation of the scatterers.[19] If the scatterers are not randomly spaced in the volume, than resonance peaks would appear in the coherent spectrum corresponding to the spacings of the scatterers.[20] For random scattering, the coherent spectrum appears as noise (called spatial variation noise).

The spatial variation noise can adversely affect the ability to estimate the shape and magnitude of the incoherent spectrum.[21] The spatial variation noise can be reduced by two means. If the gated length of the corresponding rf time signal is sufficiently long, the spatial variation noise is reduced.[18] Second, to reduce the influence of the spatial variation noise, the backscattered spectra from several independent rt time samples (denoted herein as A-lines) are spatially averaged.[5,6,17,18,21] If the interrogated scattering volume is homogeneous (uniform distribution of random, nearly identical scatterers), then samples throughout the volume can be measured and averaged.

If the interrogated volume has regions with different scattering statistics, smaller ROIs within the interrogated volume are needed to distinguish and characterize the different regions within the interrogated volume. Smaller ROIs are chosen within the interrogated volume to resolve changing

[a]Electronic mail: oelze@brl.uiuc.edu

 0001-4966/2004/115(6)/3226/9/$20.00

structure within the interrogated volume (assuming that the scatterers are much smaller than the sizes of the ROIs). The ROIs are assumed to have relative uniform scattering within the interrogated volume composed of possible nonuniform scattering.

The smaller the ROIs, the better the approximation that structure within an individual ROI is uniform. However, as the ROI becomes smaller, the number of independent samples that can be measured decreases and the length of the gate decreases. The volume interrogated by a single scan line depends on the beamwidth of the transducer and the gated length along the transducer axis.

Several studies have examined the effects of the axial gate length and windowing function on the ability to make scatterer property estimates. One study indicated that when the gated length was not large (five times the wavelength at the center frequency) the measured backscattered power spectrum did not fit the theoretical power spectrum well.[22] As the size of the gated length increased, the measured backscattered power spectrum fit the theoretical power spectrum better. Further, a better fit to the theoretical power spectrum was revealed at a gate length of 12.5 times the wavelength at the center frequency when a Hanning window was used over a rectangular window. Other studies indicated that if the length of the axial gate was larger than the pulse length, the contribution of the spatial variation noise was reduced.[18,23] As the axial gate length was reduced to the length of the pulse, it was noted that truncation errors occurred and that the length of the pulse needed to be incorporated into spectral estimates.[24] Attempts were made with limited success to correct for the small gate truncation errors using a deconvolution method.[25]

In another study, axial resolution for ROIs was optimized at a length of 10 times the wavelength of interrogation.[15] In that study, a line was fit to the backscattered power spectrum versus gated axial length using a Hanning window. The 10-wavelength ROI was chosen at the point where the slope estimates from the best-fit line first converged. The study examined the accuracy of slope estimates versus axial length but did not consider the precision in making estimates versus axial length. A similar study examined the precision limits of estimating the frequency dependence of the backscattered power spectrum versus gate length.[26] The study showed that as the gate length increased the precision of estimates improved. Further, the study did not take into account the effects of the lateral ROI size on the accuracy and precision of estimates.

The lateral ROI length and the A-line separation are other important considerations to the accuracy and precision of estimates. A rule of thumb has been that the averaged backscattered spectrum should consist of a number of A-lines sampled at a half beamwidth apart.[21,27] Some researchers have suggested spatially averaging 25 A-lines for sufficient sampling and noise reduction, while others have suggested 5–10 A-lines.[17,18] The half beamwidth center-to-center distance between A-lines is conjectured to give nearly independent samples and further reduce spatial variation noise.[21] However, no definitive rules for determining the optimal lateral ROI length and A-line center-to-center distance have been indicated.

One study examined the precision and accuracy of spectral estimation with both axial and lateral ROI size.[28] The study compared theoretical predictions of precision with experimental measurements. The study indicated that longer axial and lateral lengths gave better precision and accuracy. However, in order to determine the size of an ROI yielding a particular accuracy and precision, both the axial and lateral ROI lengths must be examined at the same time.

In the study reported herein, a technique is developed to quantify the spatial variation noise and its decrease after spatially averaging. The axial and lateral ROI length (assuming that the scatterers are much smaller than the ROI size) for making scatterer property estimates are examined to determine the optimal ROI resolution. Further, the A-line center-to-center distance is examined to determine the optimal A-line separation distance for estimating scattering properties from weakly scattering volumes. Section II describes the theory behind backscattering from weakly scattering volumes and quantification of spatial variation noise. Section III details the simulation construction and physical phantom measurements with randomly spaced glass beads. Section IV presents the results of the simulations and phantom measurements for reducing the spatial variation noise and optimizing ROI resolution. The final section (Sec. V) gives some conclusions about the study.

II. THEORY

Consider a signal of the form, $g_L(t)$, representing a backscattered time sequence from a gated length, L, in a scattering medium. The function, $g_L(t)$, is the convolution of an impulse response $h(t)$ that incorporates the electromechanical characteristics of the transducer and diffraction, and a scattering function, $r_L(t)$, from randomly spaced, nearly identical particles[20,27]

$$g_L(t) = h(t) * r_L(t). \tag{1}$$

The Fourier transform of the signal is given by

$$G_L(f) = H(f) R_L(f). \tag{2}$$

The scattering function can be written as

$$r_L(t) = s(t + 2d_1/c) + s(t + 2d_2/c) + \cdots + s(t + 2d_N/c), \tag{3}$$

where c is the speed of sound in the medium, d_i represents the individual scatterer spacings, $s(t)$ is the scattering function for a single scatterer, and N represents the number of scatterers in the interrogated volume. The interrogated volume is determined by the length of the gate, L, and the cross-sectional area of the ensonifying beam. The Fourier transform of $r_L(t)$ is given by

$$R_L(f) = S(f)[e^{-i2\pi f(2d_1/c)} + e^{-i2\pi f(2d_2/c)} + \cdots + e^{-i2\pi f(2d_N/c)}], \tag{4}$$

where $S(f)$ is the scattering spectrum. The scattering spectrum depends on the shape and the mechanical properties of the scattering particles. The backscattered power spectrum is

the magnitude squared of Eq. (2), and is given by

$$W(f)=|G_L(f)|^2=|H(f)|^2|S(f)|^2|e^{-i2\pi f(2d_1/c)} + e^{-i2\pi f(2d_2/c)}+\cdots e^{-i2\pi f(2d_N/c)}|^2. \quad (5)$$

The backscattered power spectrum can be separated into the coherent and incoherent spectra by simplifying Eq. (5)

$$W(f)=|H(f)|^2|S(f)|^2 \times\left\{\sum_{n=1}^{N} 1+\sum_{n\neq m=1}^{N} e^{-i2\pi(f/c)(d_n-d_m)}\right\}, \quad (6)$$

where the first term on the right is the incoherent spectrum and the second term is the coherent spectrum. Rearranging terms yields

$$W(f)=|H(f)|^2|S(f)|^2\left\{N+2 \times\sum_{m>n=1}^{N}\left[\frac{e^{i2\pi(f/c)(d_n-d_m)}+e^{-i2\pi(f/c)(d_n-d_m)}}{2}\right]\right\},$$

or

$$W(f)=|H(f)|^2|S(f)|^2\left\{N+2\sum_{m>n=1}^{N}\cos(k\delta_{nm})\right\}, \quad (7)$$

where $k=2\pi f/c$, $\delta_{nm}=d_n-d_m$, and the number of terms in the coherent spectrum is $[N(N-1)]/2$. For random scattering, the form of $N|S(f)|^2$ can be estimated by assuming that the incoherent spectrum is the backscattered power spectrum, while the coherent spectrum acts as noise (spatial variation noise) that reduces the accuracy and precision of the estimation technique.

If the scatterers are randomly distributed within the interrogated volume, estimates of the scatterer properties are obtained by modeling the scatterers and fitting the model to the incoherent portion of the backscattered power spectrum. Assuming the model correctly describes the scattering, the spatial variation noise reduces the accuracy and precision of the scattering property estimates. Because the spatial variation noise depends on the random spacing of the scatterers in the interrogated volume, spatially averaging the backscattered power spectra from several different, nonoverlapping interrogated volumes can reduce the spatial variation noise. When samples from nonoverlapping, interrogated volumes are averaged, the variance in some estimated parameter, $\hat{x}$, is reduced by the number of averaged samples as[21,29]

$$\mathrm{var}(\overline{\hat{x}})=\frac{\mathrm{var}(\hat{x})}{N_s}, \quad (8)$$

where N_s is the number of averaged samples and $\overline{\hat{x}}$ represents the estimate from the averaged samples.

In making backscatter measurements using ultrasound, ROIs are selected from the interrogated volume. The ROIs are constructed from gating the different A-lines that are separated by some predetermined distance. Typically, the ultrasound source/receiver scans, or is steered, laterally across the scattering medium with individual A-lines separated by a predetermined distance related to the beamwidth. A rule of thumb has been that the A-lines be separated by a half beamwidth because it was conjectured that separating by that distance gave sufficiently independent measurements for spatial variation noise reduction.[21,30] Though the half-beamwidth separation does not give truly independent samples, a further reduction of spatial variation noise can be achieved over full-beamwidth sample separation for a particular lateral ROI length.[21] The number of samples in a particular lateral ROI length is doubled for half-beamwidth separation over full-beamwidth separation. Furthermore, the larger the lateral ROI length the greater the reduction of spatial variation noise because more independent samples would then be averaged. The distance of the separated A-lines and the number of A-lines determine the lateral resolution of an ROI.

The effects of the A-line center-to-center distance and number of samples averaged can be determined by quantifying the spatial variation noise for the backscattered power spectrum. The spatial variation noise spectrum (dB) is found by dividing the averaged measured power spectrum by the impulse response and the scattering function for the medium, $N|H(f)|^2|S(f)|^2$, giving

$$W_{svn}(f)=\left|10\log_{10}\frac{\frac{1}{N_{\mathrm{avg}}}\sum_{i=1}^{N_{\mathrm{avg}}}W_i(f)}{N|H(f)|^2|S(f)|^2}\right|, \quad (9)$$

where N_{avg} is the number of measured power spectra from different A-lines that are averaged. The spatial variation noise can be quantified by taking the average of the spatial variation noise spectrum over the analysis bandwidth

$$\langle W_{svn}\rangle=\frac{1}{B}\sum_{i=1}^{B}W_{svn}(f_i), \quad (10)$$

where B is the number of samples in the bandwidth.

If two consecutive A-lines are separated by a small distance relative to the beamwidth, the spatial variation noise spectra of the two A-lines will be highly correlated. If two A-lines are compared that correspond to completely nonoverlapping scattering volumes, the correlation between the spatial variation spectra should be close to zero. The averaging of the spatial variation noise spectra of any two different A-lines from a statistically homogeneous region will result in a decrease in the overall spatial variation noise and a subsequent decrease in $\langle W_{svn}\rangle$ over the analysis bandwidth. The relative decrease in spatial variation noise was defined according to

$$\langle W_{svn}\rangle_{\mathrm{rel}}=\frac{\frac{1}{B}\sum_{j=1}^{B}\left|10\log_{10}\frac{\frac{1}{N_{\mathrm{avg}}}\sum_{i=1}^{N_{\mathrm{avg}}}W_i(f_j)}{N|H(f_j)|^2|S(f_j)|^2}\right|}{\frac{1}{B}\sum_{j=1}^{B}\left|10\log_{10}\frac{W(f_j)}{N|H(f_j)|^2|S(f_j)|^2}\right|}, \quad (11)$$

where the numerator is $\langle W_{svn}\rangle$ for N_{avg} power spectra from different A-lines and the denominator is $\langle W_{svn}\rangle$ for a single A-line. Equation (11) compares the spatial variation noise from averaging the spatial variation spectra from several A-lines to a single A-line.

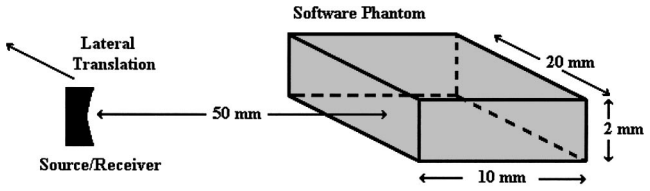

FIG. 1. Diagram of the simulated phantom with orientation and placement of the simulated source/receiver.

III. SIMULATION AND EXPERIMENTAL METHODS

The center-to-center spacing between A-lines, the number of A-lines, and the gated axial length are key factors to determining the level of spatial variation noise. There exists a trade-off between the lateral and axial length (resolution of the ROI) and the amount of spatial variation noise reduced by averaging a number of A-lines. In order to examine the trade-off between lateral and axial resolution and noise reduction, simulations from software phantoms and measurements from physical phantoms were made.

The software phantoms were constructed by first choosing a number density for each phantom of 64 mm^{-3}. A scattering volume (Fig. 1) was selected for each phantom and a number of point scatterers, number density times the phantom volume, were randomly placed in the volume. The software phantoms were assumed to be acoustically lossless. The source had a center frequency of 10 MHz and a −6-dB pulse/echo bandwidth of 5 MHz. A waveform (Fig. 2) was propagated from the source into the scattering volume at normal incidence. The source produced a Gaussian beam (laterally) with a −6-dB beamwidth of 0.6 mm. The source was weakly focused and all estimates were made within the depth of focus. Two other waveforms with beamwidths of 0.3 and 0.9 mm were simulated to evaluate whether the beamwidth was the limiting factor in lateral resolution. Each A-line was then constructed with individual point (Rayleigh) scatterers in the corresponding beam field, spherically scattering the incident pulse with the amplitude of the incident pulse and summing each scattered echo signal back at the source. Individual A-lines were constructed by translating the simulated source/receiver laterally across the length of the phantom with a step size of 25 μm.

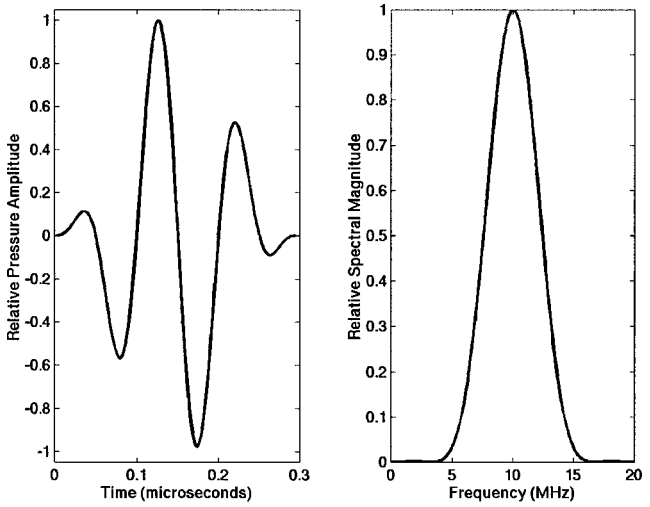

FIG. 2. Time pulse (left) and the magnitude of the frequency spectrum (right) of the simulated excitation pulse.

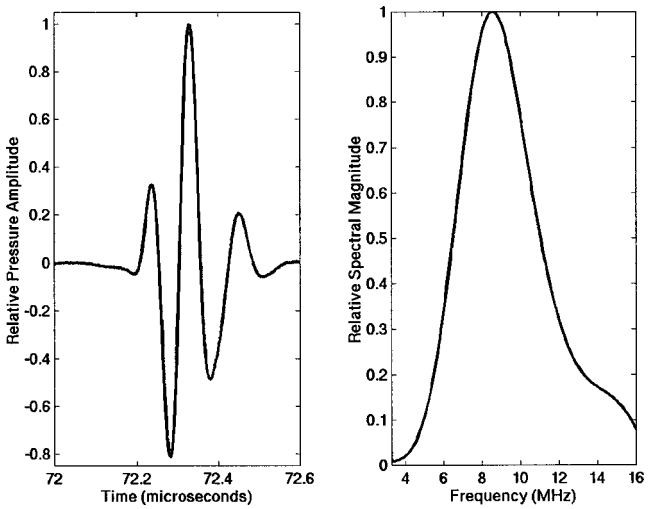

FIG. 3. Time pulse (left) and the magnitude of the frequency spectrum (right) from ultrasound reflected from a Plexiglas® reflector located at the focus of the transducer used in the physical phantom measurements.

Individual A-lines were gated using a Hanning window centered at a depth corresponding to 5 mm inside the phantom (the middle of the phantom). The backscattered power spectrum was found by taking the magnitude squared of the Fourier transform of the gated signal. The spatial variation noise in the coherent part of the backscattered spectrum was calculated from Eq. (9) with $|H(f)|^2$ equal to the power spectrum of the excitation pulse, $|S(f)|^2$ equal to the power spectrum of the point scatterers (f^4 dependence), and N equal to the number density of scatterers times the ensonified volume (cross-sectional beamwidth area times the gated length).

Measurements from two physical phantoms were made with a single-element weakly focused transducer (f number of 4) that had a center frequency of 10 MHz. The −6-dB pulse/echo bandwidth of the transducer was 6.5 MHz and the −6-dB pulse/echo beamwidth at the focus was measured to be 670 μm using the wire method.[31] Figure 3 displays an example of the incident pulse reflected from a Plexiglas® plate centered at the focus. The pulse reflected from the Plexiglas® was used as a reference pulse.[5,6,17]

In a measurement, the transducer was placed parallel to the face of the phantom so that the ultrasound would propagate normal to the surface. Both phantoms were filled with randomly placed glass beads with diameters ranging from 45 to 53 μm.[32] Phantoms A and B had measured attenuations of approximately 0.5 and 0.65 dB/MHz/cm over the range of 5–12 MHz, respectively. The number density of phantom A was close to half that of phantom B. The phantoms were scanned laterally 2 cm in length along their surface with a step size of 25 μm between each scan line (A-line). For each A-line, the backscattered signal was temporally averaged for 300 realizations to reduce any electronic noise associated with the measurement.

Individual A-lines were gated using a Hanning window of variable lengths with the edge at a depth corresponding to 2 mm inside the phantom. The backscattered power spectrum

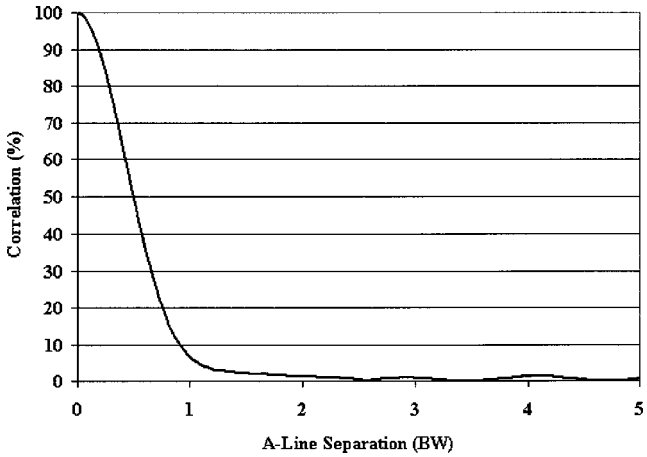

FIG. 4. Percent correlation of the spatial variation noise spectra from A-lines separated by varying distances (simulations). The line represents the average of 40 samples.

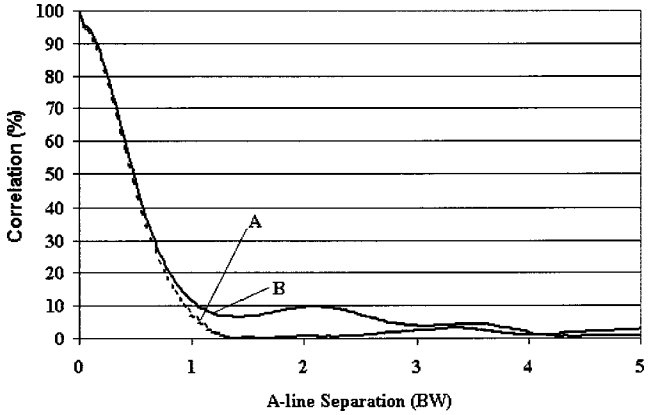

FIG. 5. Percent correlation of the spatial variation noise spectra from A-lines separated by varying distances from the physical phantoms. Each plotted line represents the average of 40 samples. Correlation lines were plotted for the two phantoms, ---, phantom A; ———, phantom B.

was found by taking the magnitude squared of the Fourier transform of the gated signal. The backscattered power spectrum was then multiplied by a frequency-dependent attenuation-compensation function.[27] The spatial variation noise spectra from the phantom measurements were calculated from Eq. (9). $|H(f)|^2$ was given by the power spectrum of the reference pulse, $|S(f)|^2$ was determined by the theory of Faran[33] for glass beads of diameter 49 μm, and N was found from the acoustic concentration determined using the MASD method.[5]

IV. SIMULATION AND EXPERIMENTAL RESULTS

The percent correlation at zero lag between the spatial variation noise spectra of two A-lines versus the A-line separation distance was determined for both the simulated phantoms and the physical phantoms according to

$$C(\%) = \frac{\Sigma_{i=1}^{B} W^*_{svn_1}(f_i) W_{svn_2}(f_i)}{\Sigma_{i=1}^{B} |W_{svn_1}(f_i)|^2} \times 100\%, \tag{12}$$

where B represents the number of sampled points in the analysis bandwidth and the two lines are represented by the subscripts 1 and 2, respectively. The center-to-center distance was normalized by dividing by the −6-dB beamwidth of the source/receiver. Figure 4 shows the percent correlation between the spatial variation noise spectra of two A-lines versus the center-to-center distance (in beamwidths, BW) for the simulated phantoms. The correlation steadily decreased as the center-to-center distance increased until the A-line center-to-center distance was about 1 beamwidth. The correlation at about 1 beamwidth began to level off to near zero. The reason for the correlation decreasing and then leveling off at a separation of near 1 beamwidth is that the compared A-lines represented nearly independent scattering volumes.

Similarly, Fig. 5 shows the percent correlation between the spatial variation noise spectra of two A-lines versus the A-line separation distance for the physical phantom measurements. In the phantom measurements, the correlation did not reach its minimum value until after the A-line separation distance exceeded the −6-dB pulse/echo beamwidth. Similar to the simulation phantoms, the correlation appeared to level off after the A-line separation distance exceeded 1 beamwidth.

The next set of measurements evaluated the decrease in $\langle W_{svn} \rangle_{\text{rel}}$ due to lateral length of the ROI. Typically, an ROI is chosen within the interrogated volume and the ROI is made up of several gated A-lines. The smaller the A-line separation distance, the more A-lines are included in a ROI. Furthermore, the larger the lateral length of the ROI, the more independent A-line samples that are included in the ROI and the greater decrease in $\langle W_{svn} \rangle_{\text{rel}}$.

Figures 6 and 7 show the decrease of $\langle W_{svn} \rangle_{\text{rel}}$ in the simulated phantoms and the physical phantoms, respectively, versus the lateral ROI length for several A-line separation distances. In both figures, $\langle W_{svn} \rangle_{\text{rel}}$ decreased with increased lateral ROI length and appeared to level off at a lateral ROI size of 15 to 20 BW for the phantom measurements. To compare the decrease in $\langle W_{svn} \rangle_{\text{rel}}$ versus lateral ROI distance for both simulated and physical phantoms, the distance at which $\langle W_{svn} \rangle_{\text{rel}}$ decreased to 1/e of its value for a single, unaveraged A-line sample was used. For the case of the simulated phantom, the 1/e decrease of $\langle W_{svn} \rangle_{rel}$ occurred at a lateral ROI size of around 5 BW and the 1/e value for the

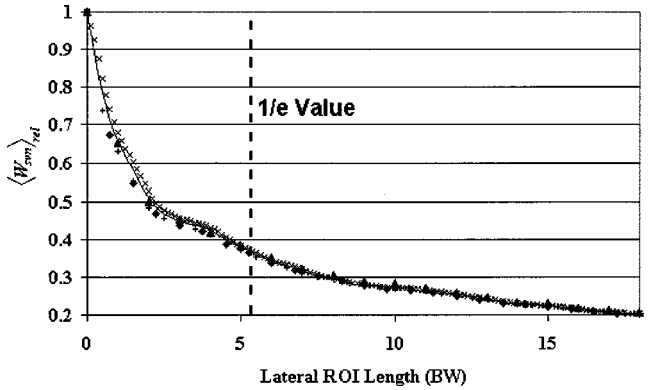

FIG. 6. $\langle W_{svn} \rangle_{\text{rel}}$ determined from the simulated phantoms over the frequency bandwidth 6–14 MHz relative to $\langle W_{svn} \rangle_{\text{rel}}$ for a single A-line. The number of averaged A-lines depends on the lateral ROI length and the A-line separation distances, ———, 0.125 BW; ×, 0.25 BW; +, 0.50 BW; ◆, 0.75 BW; ▲, 1.0 BW.

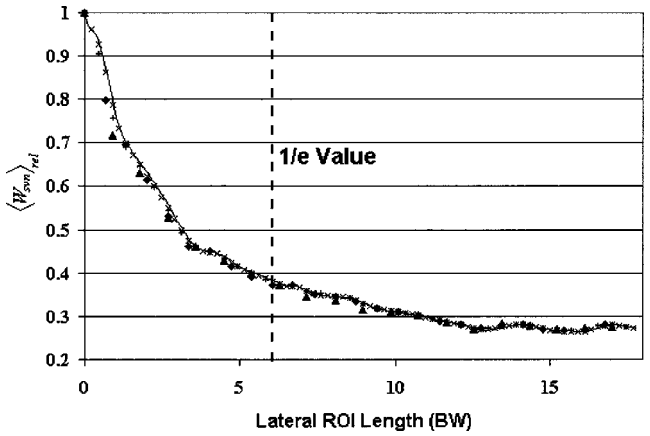

FIG. 7. $\langle W_{svn}\rangle_{\text{rel}}$ measured from the physical phantoms over the frequency bandwidth 6–14 MHz relative to $\langle W_{svn}\rangle_{\text{rel}}$ for a single A-line. The number of averaged A-lines depends on the lateral ROI length and the A-line separation distances, ———, 0.125 BW; ×, 0.25 BW; +, 0.50 BW; ♦, 0.75 BW; ▲, 1.0 BW.

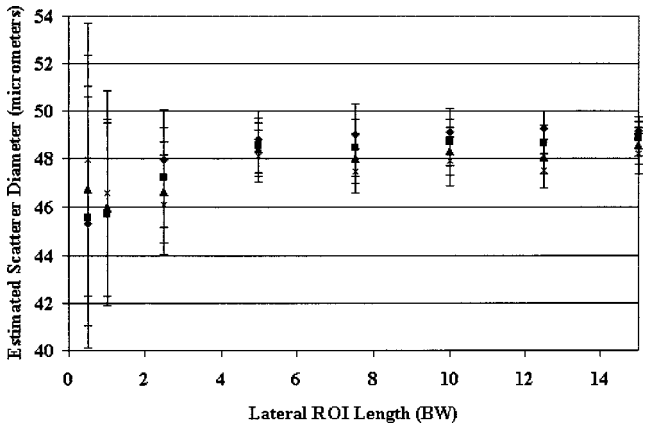

FIG. 8. Estimates of the average scatterer size of glass beads. The error bars represent the standard deviation of six measurements from phantom A and six measurements from phantom B with ROIs of the same size and same depth in the phantoms.

physical phantom measurements occurred at around 6 BW. In the simulations and the physical phantom measurements, the A-line separation distance did not appear give additional decreases in $\langle W_{svn}\rangle_{\text{rel}}$.

Figures 6 and 7 indicated that the most important factor to reducing spatial variation noise was not the A-line separation distance but rather the lateral length of the ROI. Averaging the backscattered spectra from any two different A-lines, whether they are from independent samples or not, will decrease the spatial variation noise. The lateral ROI length was the most important factor in spatial variation noise reduction; however, using A-lines with smaller separation distances means that you have a greater sampling over the lateral ROI length. Furthermore, any electronic noise in the backscattered spectrum will have little correlation from one A-line to the next, no matter the separation distance. The advantage to averaging the backscattered power spectra from many A-lines, because the A-lines separation distance is small, is that the electronic noise is reduced more than averaging the backscattered power spectra from just a few A-lines. In at least one study, improvement in scatterer property estimates was indicated by choosing smaller A-line separation distances.[34]

Figure 8 reveals the importance of the lateral ROI length for decreasing the spatial variation noise. The average size of the scatterers in the phantoms was estimated from the backscattered power spectrum using the MASD estimation technique and the theory of Faran.[5,33] The backscattered power spectrum was measured by selecting ROIs in the physical phantoms with axial lengths of 4 mm and varying the lateral ROI lengths. The analysis bandwidth used for the estimates was from 5–12 MHz. The analysis bandwidth corresponded to a ka range of 0.5 to 1.2, which has been measured to be the optimal range for estimating glass bead sizes.[6]

Estimates of glass bead sizes indicated that both accuracy and precision were affected by the lateral ROI length and not significantly by the A-line separation distance. The estimates of average glass bead size converged as the lateral ROI length approached 5 BW (Fig. 8). Furthermore, the error bars indicate that the precision of the estimates increased as the lateral ROI length increased up to a lateral ROI length of 5 BW. Beyond a lateral ROI length of 5 BW, no significant gains were made in accuracy and precision of the estimates.

Measurements of the spatial variation noise with source/receivers having different beamwidths indicated the optimal lateral ROI length in terms of BW was independent of the width of the beam. $\langle W_{svn}\rangle_{\text{rel}}$ was calculated at an A-line separation of 0.25 BW with beams of lateral length of 0.3, 0.6, and 0.9 mm. Figure 9 shows the relative spatial variation noise decrease in $\langle W_{svn}\rangle_{\text{rel}}$ as the lateral ROI length increased. The 1/e decrease in the spatial variation noise occurred in each measurement at a lateral ROI length of approximately 5 BW. The measurements indicate the optimal lateral ROI resolution is independent of the beamwidth of the source/receiver.

The decrease in $\langle W_{svn}\rangle_{\text{rel}}$ was also examined versus the axial gate length. Figure 10 shows a plot of the axial length in pulse lengths (PLs) versus the 1/e lateral ROI distance (BW) at which $\langle W_{svn}\rangle_{\text{rel}}$ decreased to 1/e of the maximum

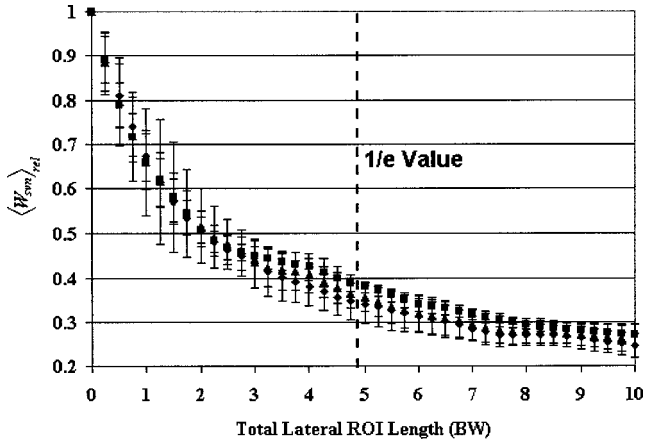

FIG. 9. $\langle W_{svn}\rangle_{\text{rel}}$ measured from the physical phantoms over the frequency bandwidth 6–14 MHz relative to $\langle W_{svn}\rangle_{\text{rel}}$ for a single A-line versus the lateral ROI length. The measurements were made with simulated source/receivers having beamwidths defined as, ♦, 0.3 mm; ■, 0.6 mm; ▲, 0.9 mm with A-line separation of 0.25 BW. The error bars represent the standard deviation about the mean of six independent measurements.

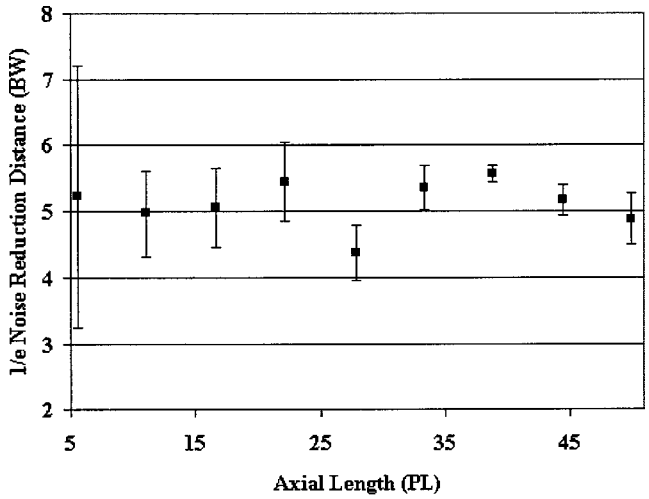

FIG. 10. The lateral ROI length where $\langle W_{svn} \rangle_{\text{rel}}$ reduces by 1/e of the value relative to $\langle W_{svn} \rangle_{\text{rel}}$ for a single A-line versus the axial gate length. The error bars represent the standard deviation of four simulated phantoms.

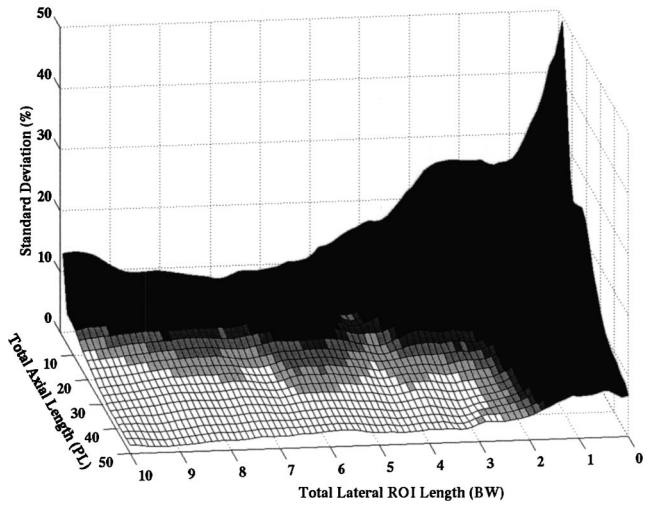

FIG. 12. Standard deviation of estimates of frequency dependence of backscattered power spectrum from randomly placed point scatterers as a percent of actual value versus axial and lateral ROI length.

value. The axial gate length did not appear to effect the average lateral ROI distance at which $\langle W_{svn} \rangle_{\text{rel}}$ was decreased to 1/e of the initial value. The dominant factor in decreasing $\langle W_{svn} \rangle_{\text{rel}}$ was the lateral ROI length. However, at smaller gate lengths the standard deviation for estimating the 1/e decrease in $\langle W_{svn} \rangle_{\text{rel}}$ was much greater. The axial gate length will affect the ability to make accurate and precise estimates. The spatial variation noise explains the effects of the lateral ROI length on the accuracy and precision of scatterer property estimates, but may not be the best measure for determining the optimal axial length for an ROI. Other effects than the spatial variation noise contribute to the loss of accuracy and precision at smaller axial gate lengths.[25]

The next simulation examined the accuracy and precision of parametrizing the frequency dependence of the backscattered power spectrum versus different lateral and axial ROI lengths affected. Point scatterers have frequency dependence to the fourth power for backscatter. Figures 11 and 12, respectively, show the accuracy and precision of estimating the frequency dependence of point scatterers versus different sizes of ROIs. The best accuracy and precision of estimates were obtained when the axial gate length and lateral ROI length were the largest. However, if smaller ROIs are desired to improve resolution and to increase the likelihood that the ROI contains uniform scattering statistics, then smaller ROIs that still retain good accuracy and precision of estimates should be chosen. For example, if the smallest possible ROI is desired while still retaining within 5% accuracy and precision, an ROI of 15 PLs times 5 BWs would fit.

The importance of the axial and lateral length of an ROI to the accuracy and precision of estimates can be seen from the phantom measurements (Figs. 13 and 14, respectively). The average size of the scatterers in the phantoms was estimated from the backscattered power spectrum using the MASD estimation technique and the theory of Faran.[5,33] The backscattered power spectrum was measured by selecting ROIs in the physical phantoms with variable axial and lateral

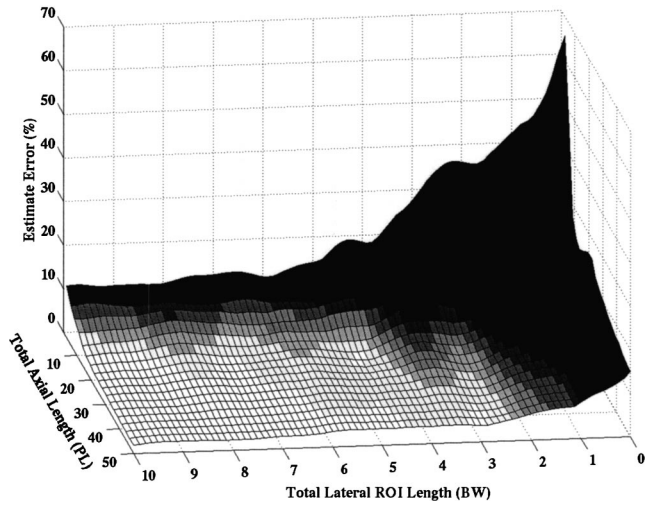

FIG. 11. Percent error between estimates of frequency dependence of backscattered power spectrum from randomly placed point scatterers and actual value (f^4) for point scatterers versus axial and lateral ROI length.

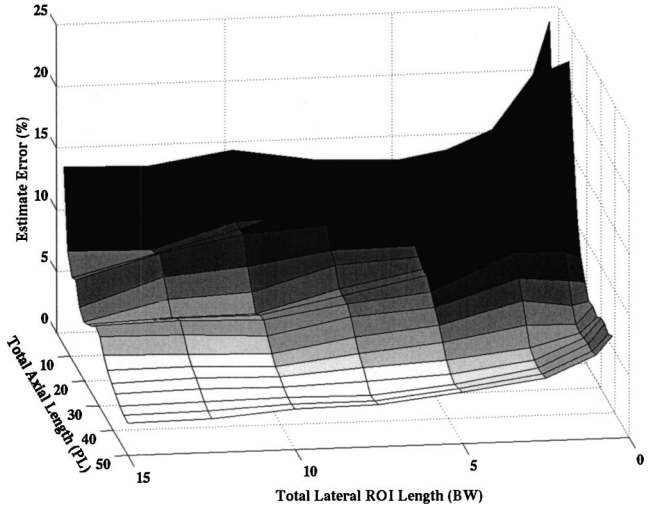

FIG. 13. Percent error between estimates of glass bead size from the backscattered power spectrum and actual values versus axial and lateral ROI length.

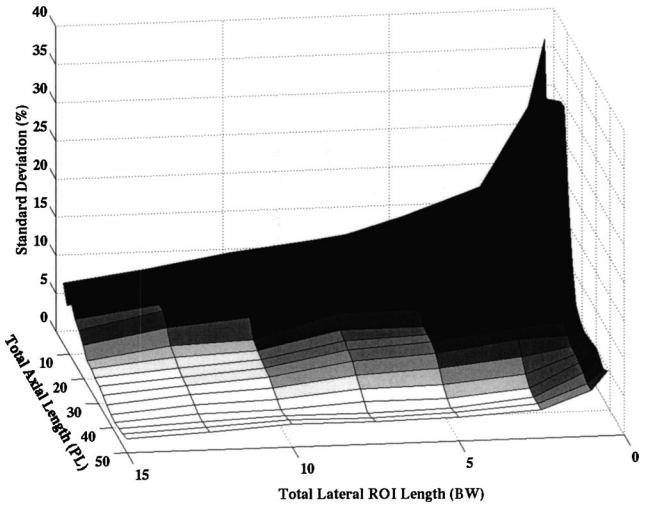

FIG. 14. Standard deviation of glass bead size estimates from the backscattered power spectrum as a percent of actual value versus axial and lateral ROI length.

ROI lengths. The analysis bandwidth used for the estimates was from 5–12 MHz.

Estimates of glass bead sizes indicated that the lateral and axial ROI length affected both accuracy and precision. Small axial gate lengths led to the largest inaccuracies in the estimate of scatterer size (Fig. 13). Errors of less than 10% occurred with axial gate lengths equal to or larger than 12 PLs and lateral ROI lengths of 5 BW. Smaller lateral lengths can be used with equivalent errors by using larger axial gate lengths. The precision of the estimates improved as the ROI area increased (Fig. 14). The standard deviation of less than 5% occurred when the ROI had an axial length of around 15–20 PLs and a lateral length of 5 BWs.

In order to obtain accurate and precise estimates, it must be noted that the number of samples within the lateral ROI length must be large enough. The importance of obtaining enough samples in the lateral ROI length was indicated from the 1-beamwidth separation data (Figs. 6 and 7). At the 5 BW, lateral ROI length line, 6 A-lines at the 1-full-beamwidth separation distance were sampled. The data point at the zero lateral ROI length value could be thought of as sampling one independent sample over a lateral ROI length of 5 BW. The data point at the lateral ROI length of 1 beamwidth could be thought of as sampling two independent samples over a lateral ROI length of 5 BW. The same goes for each data point up to the lateral ROI length of 5 BW (six independent samples). The data indicate that to get the best accuracy at the lateral ROI length of 5 BW there must minimally be an A-line separation of 1 beamwidth, with 6 being the total number of samples. The A-line separation distance can be as small as desired but the upper bound should be at most 1 beamwidth.

V. DISCUSSION

When making estimates of scatterer properties from the backscattered spectra of weakly scattering volumes, the sizes of ROIs selected are important to obtaining good estimates. In tissues it is especially important to minimize the ROI size because of possible variations throughout a larger volume. ROIs are chosen within the interrogated volume under the assumption that within the individual ROIs, the scattering properties are statistically uniform while in the larger volume, variation in the scattering properties may exist. Smaller ROIs allow for regions with different scattering statistics to be resolved in the overall volume. However, if the ROIs are too small, the accuracy and precision of scattering estimates suffer.

Optimizing the resolution (ROI size) with regards to the accuracy and precision of spectral estimates is important to tissue characterization. Typically, the rule of thumb has been that backscattered spectra should be averaged from A-lines separated by a distance of a half beamwidth. The more A-lines (longer lateral ROI length) the better the spectral characterization. Further, longer gate lengths were revealed to produce better estimates.

Results from simulation and physical phantom experiments indicated that the separation distance of the A-lines was not as important a factor in determining the accuracy and precision of scattering estimates as the lateral ROI length. However, when optimizing for ROI size, the separation distance of A-lines in the ROI should be at most 1 beamwidth. Choosing A-line separation distances smaller than 1 beamwidth can reduce the electronic noise further.

The key factor in reducing spatial variation noise and improving the accuracy and precision of scattering estimates was the overall axial and lateral lengths of the ROI. The simulations and phantom measurements indicated the optimal lateral and axial length, where estimate accuracy was consistently within 10% and precision within 5% of actual values, occurred at 4 to 5 beamwidths and 15 to 20 pulse lengths, respectively. Optimally, the results of the simulation and phantom experiments showed that the total lateral length of an ROI should be 5 BW. The total lateral length of 5 BW represents the length where the spatial variation noise was reduced by 1/e through averaging of the backscattered spectra from the individual A-lines. Furthermore, the lateral length size of 5 BW represented the length where the best accuracy and precision of glass bead estimates from the physical phantoms were reached. There was minimal advantage to increasing the ROI size beyond 4 to 5 beamwidths laterally and 15–20 pulse lengths axially. Increasing the size of the ROI gave some improvement in accuracy and precision, but such gains may be offset by tissue inhomogeneity. Similar accuracy and precision could be achieved by increasing either the axial length and decreasing the lateral length, or vice versa. The A-line separation distance should be less than or equal to 1 beamwidth, with smaller A-lines separation distances typically giving further reductions in electronic noise.

ACKNOWLEDGMENTS

Supported by NIH CA 079179 and NIH F32 CA96419 to M.L.O.

[1] D. Nicholas, ''Evaluation of backscattering coefficients for excised human tissues: Results, interpretation, and associated measurements,'' Ultrasound Med. Biol. **8**, 17–28 (1982).

[2] E. J. Feleppa, F. L. Lizzi, D. J. Coleman, and M. M. Yaremko, ''Diagnostic spectrum analysis in ophthalmology: A physical perspective,'' Ultrasound Med. Biol. **12**, 623–631 (1986).
[3] F. L. Lizzi, M. Ostromogilsky, E. J. Feleppa, M. C. Rorke, and M. M. Yaremko, ''Relationship of ultrasonic spectral parameters to features of tissue microstructure,'' IEEE Trans. Ultrason. Ferroelectr. Freq. Control **33**, 319–329 (1986).
[4] D. K. Nassiri and C. R. Hill, ''The use of angular scattering measurements to estimate structural parameters of human and animal tissues,'' J. Acoust. Soc. Am. **87**, 179–192 (1990).
[5] M. F. Insana, R. F. Wagner, D. G. Brown, and T. J. Hall, ''Describing small-scale structure in random media using pulse–echo ultrasound,'' J. Acoust. Soc. Am. **87**, 179–192 (1990).
[6] M. F. Insana and T. J. Hall, ''Parametric ultrasound imaging from backscatter coefficient measurements: Image formation and interpretation,'' Ultrason. Imaging **12**, 245–267 (1990).
[7] M. F. Insana, J. G. Wood, and T. J. Hall, ''Identifying acoustic scattering sources in normal renal parenchyma from the anisotropy in acoustic properties,'' Ultrasound Med. Biol. **18**, 587–599 (1992).
[8] K. K. Shung and G. A. Thieme, *Ultrasonic Scattering in Biological Tissues* (CRC Press, Boca Raton, 1993).
[9] M. F. Insana, T. J. Hall, J. G. Wood, and Z.-Y. Yan, ''Renal ultrasound using parametric imaging techniques to detect changes in microstructure and function,'' Invest. Radiol. **28**, 720–725 (1993).
[10] M. F. Insana, ''Modeling acoustic backscatter from kidney microstructure using an anisotropic correlation function,'' J. Acoust. Soc. Am. **97**, 649–655 (1995).
[11] T. J. Hall, M. F. Insana, L. A. Harrison, and G. G. Cox, ''Ultrasonic measurement of glomerular diameters in normal adult humans,'' Ultrasound Med. Biol. **22**, 987–997 (1996).
[12] E. J. Feleppa, T. Liu, A. Kalisz, M. C. Shao, N. Fleshner, and V. Reuter, ''Ultrasonic spectral-parameter imaging of the prostate,'' Int. J. Imaging Syst. Technol. **8**, 11–25 (1997).
[13] F. L. Lizzi, M. Astor, T. Liu, C. Deng, D. J. Coleman, and R. H. Silverman, ''Ultrasonic spectrum analysis for tissue assays and therapy evaluation,'' Int. J. Imaging Syst. Technol. **8**, 3–10 (1997).
[14] R. M. Golub, R. E. Parsons, B. Sigel, E. J. Feleppa, J. Justin, H. A. Zaren, M. Rorke, J. Sokil-Melgar, and H. Kimitsuki, ''Differentiation of breast tumors by ultrasonic tissue characterization,'' J. Ultrasound Med. **12**, 601–608 (1993).
[15] K. A. Topp, J. F. Zachary, and W. D. O'Brien, Jr., ''Quantifying B-mode images of *in vivo* rat mammary tumor with frequency dependence of backscatter,'' J. Ultrasound Med. **20**, 605–612 (2001).
[16] M. L. Oelze, J. F. Zachary, and W. D. O'Brien, Jr., ''Parametric imaging of rat mammary tumors *in vivo* for the purposes of tissue characterization,'' J. Ultrasound Med. **21**, 1201–1210 (2002).
[17] F. L. Lizzi, M. Greenbaum, E. J. Feleppa, M. Elbaum, and D. J. Coleman, ''Theoretical framework for spectrum analysis in ultrasonic tissue characterization,'' J. Acoust. Soc. Am. **73**, 1366–1373 (1983).
[18] E. L. Madsen, M. F. Insana, and J. A. Zagzebski, ''Method of data reduction for accurate determination of acoustic backscatter coefficients,'' J. Acoust. Soc. Am. **76**, 913–923 (1984).
[19] J. F. Chen, E. L. Madsen, and J. A. Zagzebski, ''A method for determination of frequency-dependent effective number density,'' J. Acoust. Soc. Am. **95**, 77–85 (1994).
[20] K. A. Wear, R. F. Wagner, M. F. Insana, and T. J. Hall, ''Application of autoregressive spectral analysis to cepstral estimation of mean scatterer spacing,'' IEEE Trans. Ultrason. Ferroelectr. Freq. Control **40**, 50–58 (1993).
[21] R. Kuc, ''Bounds on estimating the acoustic attenuation of small tissue regions from reflected ultrasound,'' Proc. IEEE **73**, 1159–1168 (1985).
[22] J. F. Chen, J. A. Zagzebski, and E. L. Madsen, ''Tests of backscatter coefficient measurement using broadband pulses,'' IEEE Trans. Ultrason. Ferroelectr. Freq. Control **40**, 603–607 (1993).
[23] M. F. Insana, E. L. Madsen, T. J. Hall, and J. A. Zagzebski, ''Tests of the accuracy of a data reduction method for determination of acoustic backscatter coefficients,'' J. Acoust. Soc. Am. **79**, 1230–1236 (1986).
[24] M. Ueda and Y. Ozawa, ''Spectral analysis of echoes for backscattering coefficient measurement,'' J. Acoust. Soc. Am. **77**, 38–47 (1985).
[25] M. Akita and M. Ueda, ''The effect of windowing on spectral estimation of echoes scattered by a random medium,'' J. Acoust. Soc. Am. **83**, 1243–1248 (1988).
[26] K. A. Wear, ''Fundamental precision limitations for measurements of frequency dependence of backscatter: Applications in tissue-mimicking phantoms and trabecular bone,'' J. Acoust. Soc. Am. **110**, 3275–3283 (2001).
[27] M. L. Oelze and W. D. O'Brien, Jr., ''Frequency-dependent attenuation-compensation functions for ultrasonic signals backscattered from random media,'' J. Acoust. Soc. Am. **111**, 2308–2319 (2002).
[28] H. J. Huisman and J. M. Thijssen, ''Precision and accuracy of acoustospectrographic parameters,'' Ultrasound Med. Biol. **22**, 855–871 (1996).
[29] A. Oppenheim and R. Schafer, *Digital Signal Processing* (Prentice Hall, Englewood Cliffs, NJ, 1975).
[30] F. Padilla, F. Peyrin, and P. Laugier, ''Prediction of backscatter coefficient in trabecular bones using a numerical model of three-dimensional microstructure,'' J. Acoust. Soc. Am. **113**, 1122–1129 (2003).
[31] K. Raum and W. D. O'Brien, Jr., ''Pulse–echo field distribution measurement technique for high-frequency ultrasound sources,'' IEEE Trans. Ultrason. Ferroelectr. Freq. Control **44**, 810–815 (1997).
[32] E. L. Madsen, F. Dong, G. R. Frank, B. S. Garra, K. A. Wear, T. Wilson, J. A. Zagzebski, H. L. Miller, K. Shung, S. H. Wang, E. J. Feleppa, T. Liu, W. D. O'Brien, Jr., K. A. Topp, N. T. Sanghvi, A. V. Zaitsev, T. J. Hall, J. B. Fowlkes, O. D. Kripfgans, and J. G. Miller, ''Interlaboratory comparison of ultrasonic backscatter, attenuation, and speed measurements,'' J. Ultrasound Med. **18**, 615–631 (1999).
[33] J. J. Faran, Jr., ''Sound scattering by solid cylinders and spheres,'' J. Acoust. Soc. Am. **23**, 405–418 (1951).
[34] M. E. Anderson, M. S. C. Coo, and G. E. Trahey, ''*In vivo* breast tissue backscatter measurements with 7.5- and 10-MHz transducers,'' Ultrasound Med. Biol. **27**, 75–81 (2001).